In situ study of surface species and structure over Oxide-Derived Copper Catalysts for Electrochemical CO2 Reduction

Chunjun Chen
Institute of Chemistry, Chinese Academy of Sciences
Xupeng Yan
Institute of Chemistry
Yahui Wu
Institute of Chemistry
Shoujie Liu
Chemistry and Chemical Engineering of Guangdong Laboratory
Xiaofu Sun
Institute of Chemistry, Chinese Academy of Sciences
Qinggong Zhu
Institute of Chemistry, Chinese Academy of Sciences https://orcid.org/0000-0001-8730-8486
Rongjuan Feng
CAS Key Laboratory of Standardization and Measurement for Nanotechnology, CAS Center for Excellence in Nanoscience, National Center for Nanoscience and Technology, Beijing 100190, P. R. China
Tianbin Wu
Institute of Chemistry, The Chinese Academy of Sciences
Qingli Qian
Institute of Chemistry https://orcid.org/0000-0002-1142-8948
Huizhen Liu
Institute of Chemistry
Lirong Zheng
Chinese Academy of Sciences
Jing Zhang
Institute of high energy physics, chinese academy of science
Buxing Han (hanbx@iccas.ac.cn)
Institute of Chemistry, Chinese Academy of Sciences

Article

Keywords: Surface-enhanced Raman Spectroscopy, Operando X-ray Absorption Spectroscopy, 18O Isotope Labeling, Density Functional Theory

Posted Date: September 25th, 2020

DOI: https://doi.org/10.21203/rs.3.rs-74951/v1

Version of Record: A version of this preprint was published at Chemical Science on January 1st, 2021.
See the published version at https://doi.org/10.1039/D1SC00042J.

Abstract

The oxide-derived copper (OD-Cu) has been discovered as effective catalyst for electroreduction of CO_2 to C2+ products. The real structure of the OD-Cu and surface species in the reaction process are interesting phenomena, which are not clear now. Herein, in situ surface-enhanced Raman spectroscopy (SERS), operando X-ray absorption spectroscopy (XAS), ^{18}O isotope labeling experiments, and density functional theory were employed to investigate the surface speciation and structure of the OD-Cu catalysts during CO_2 electroreduction. It was found that the OD-Cu catalysts were reduced to metallic Cu(0) in the reaction. CuOx species existed on the catalyst surfaces during CO_2RR, which resulted from the chemisorption of CO_2 instead of active sites of the catalyst. After removing potential, Cu_2O was formed on the surface of the catalyst by reaction of Cu and H_2O. It was also found that Cu (100) facet can be enhanced by redox cycling treatment of the catalyst, leading to outstanding performance of the catalyst. The Faradaic efficiency(FE) for C2+ products reached up to 83.8% at current density of 341.5 mA•cm^{-2} at -0.9 V vs RHE. The findings of this work are very interesting knowledge in the area in electrochemical reduction of CO_2. The work also demonstrates advantage and necessity of in situ experimental methods in exploring the interesting phenomena in the process of CO_2RR.

Introduction

Electrochemical CO_2 reduction reaction (CO_2RR) has received wide attention, which can not only reduce CO_2 into chemical fuels and feedstocks, but also provide an energy storage solution to the renewable energy sources.[1-5] Especially, multi-carbon (C2+) products are much more attractive, due to the high energy density and high economic value.[6-10] However, the activity and selectivity for C2+ products are severely limited by slow kinetics of C-C coupling step, which involves intricate multiple proton and electron transfer.[11-15] Designing highly active catalysts for C2+ products and confirming the active sites are crucial to promoting the development of this area.

The Cu-based catalysts are the most promising electrocatalysts for converting CO_2 to C2+ products,[16-20] especially the oxide-derived Cu (OD-Cu).[21-23] Studies using ambient-pressure X-ray photoelectron spectroscopy, electron energy-loss spectroscopy and ex situ energy-dispersive X-ray spectroscopy have shown that oxide species in OD-Cu play the crucial role in activating CO_2 and C-C coupling.[24-26] However, it is well-known that the Cu oxide and hydroxide species are unstable at negative potentials during CO_2RR. In addition, most of the characterization on CuO_x species are based on ex situ methods, and it is difficult to study the structure and valence of catalysts at the reaction condition, due to the reduced Cu can be oxidized very rapidly even in trace amounts of O_2 atmosphere. Thus the real role of CuOx species in OD-Cu on promoting CO_2RR was controversial. In previous reports,[27-28] massive efforts have been focused on the presence or absence of Cu oxides, however, how the Cu oxides were retained or formed

during CO_2RR was not clear. And the comprehensive knowledge of the CuOx species is crucial to understand their roles on promoting CO_2RR.

Moreover, the surface structure of catalysts often plays crucial role for producing C2+ products.[29-31] Experimental studies suggested that the grain boundaries, low coordination environment and active crystal facets can alter the CO adsorption and C-C coupling step during CO_2RR.[32-35] These factors are often associated rather than independent. For example, the active facets tend to be exposed on the surface in the region near grain boundaries, as the grain boundaries could stabilize the facets with high surface energy according to the solid-state mechanical studies.[36-37] Thus, the surface structure should also be comprehensively studied at the reaction condition.

In this work, the surface species of the OD-Cu catalysts were systematically studied via in situ surface-enhanced Raman spectroscopy (SERS), operando X-ray absorption spectroscopy (XAS), and isotope labeling experiments. It was found that the CuO_x species existed on the Cu surfaces during CO_2RR, and they were from the chemisorption of CO_2 on metallic Cu(0) at negative potential rather than the residual oxides. The presence of the CuO_x species was unlikely the factor for enhancing C2+ products. The experimental and DFT studies indicate that the generated active facets in the redox cycling treatment played the key role for highly efficient C2+ products production.

Results

Synthesis and characterization of Cu-nr and Cu-nr-OR. Two different OD-Cu catalysts with similar morphology were studied in this work. Firstly, the Cu nanorods (Cu-nr) was first prepared by electroreduction of CuO nanorods. In order to eliminate the influence of morphology on acivity of OD-Cu as much as possible, another OD-Cu catalyst was prepared by simple redox cycling treatment of Cu-nr. The Cu-nr oxide (Cu-nr-O) was prepared by oxidation of Cu-nr in 1.0 M KOH solution, then the reduced Cu-nr-O (Cu-nr-OR) was obtained by electroreduction of the Cu-nr-O (Supporting Information, Figure S1). The obtained Cu-nr had a diameter of about 40 nm (Supporting Information, Figure S2), and they exhibited cross-linked architecture. Scanning electron microscope (SEM) and transmission electron microscopy (TEM) suggested that the Cu-nr-OR also exhibited the nanorod morphology, which was similar to the Cu-nr (Figure 1A, 1B). From the high-resolution TEM image (Figure 1C and Supporting Information, Figure S3), the corresponding lattice distance of CuO (001), Cu_2O (111) and Cu (111) were observed on Cu-nr-OR, which may be due to the oxidation of Cu at the surface by air, because the TEM study was carried out at ex situ mode.

In order to trace the detailed information regarding Cu speciation, X-ray absorption spectroscopy (XAS) was used to explore the electronic structures of the catalysts. The X-ray absorption near edge structure (XANES) spectroscopy (Figure 1D) showed that the pre-edge peak of Cu-nr-O was close to Cu_2O. The oscillation k3χ (k) functions of Cu-nr-O (Supporting Information, Figure S4) indicated that the low k region

was similar to Cu_2O and high k region was similar to Cu, indicating both Cu_2O and Cu exsited in the Cu-nr-O. According to extended X-ray absorption fine structure (EXAFS) spectroscopy (Figure 1E), Cu-O and Cu-Cu coordination peaks were observed in Cu-nr-O, implying that a portion of Cu was oxided to Cu_2O. In contrast, for the Cu-nr-OR, only peaks corresponding to metallic Cu were observed, indicating that the Cu_2O of Cu-nr-O was reduced to metallic Cu after the electroreduction.

Electrocatalytic performance of CO_2 reduction over Cu-nr and Cu-nr-OR. The electrocatalytic performance of the catalysts were evaluated in a flow cell, as reported in our previous work.[38] The gas chromatography (GC) and nuclear magnetic resonance (NMR) spectroscopy were used to analyze the gaseous and liquid products, respectively (Supporting Information, Figure S5). For Cu-nr-OR, the FE of C2+ products (FE_{C2+}) could reach up to 83.8% with a current density of 341.5 mA•cm^{-2} at -0.9 V vs RHE (Figure 2A), which was among the best values reported up to date (Table S1). In contrast, the FE_{C2+} for the Cu-nr was 64.6% at -0.9 V vs. RHE with a current density of 271.2 mA•cm^{-2} (Figure 2B). The partial current density of C2+ products over Cu-nr-OR could reach 286.2 mA•cm^{-2} at -0.9 V vs. RHE, which is about 1.6 times of that over Cu-nr (Figure 2C). These results indicate that Cu-nr-OR had better performance than the Cu-nr for generating C2+ products. The other products generated in the reaction are listed in Supporting Information (Figure S6). The long-term operation was conducted at -0.9 V vs. RHE over Cu-nr-OR to elucidate the electrode stability. There was no obvious decay in both current density and FE of the products during 24 h (Figure 2D).

In order to verify that the products were derived from CO_2, the electrolysis experiment was conducted using isotope labeled $^{13}CO_2$ over Cu-nr-OR. From ^{1}H NMR spectra (Supporting Information, Figure S7), we can know that the H signal of the products splited into two group peaks, which results from the coupling effect of H-^{13}C atom. These results indicate that CO_2 is the only source of carbon in the products.

Discussion

The intrinsic reasons for the enhanced activity and selectivity for CO_2 reduction to C2+ products over Cu-nr-OR were further investigated. The electrochemical active surface areas (ECSA) of Cu-nr and Cu-nr-OR were estimated by measuring double layer capacitance. We can observe that the ECSA of Cu-nr-OR was similar to that of the Cu-nr (Supporting Information, Figure S8). Thus, the improved C2+ products generation resulted not mainly from the slight change of the ECSA. Furthermore, electrochemical impedance spectroscopy (EIS) was carried out to measure the charge transfer resistance (R_{ct}) for Cu-nr and Cu-nr-OR. The Cu-nr-OR showed similar interfacial R_{ct} with Cu-nr(Supporting Information, Figure S9).

Due to the selectivity of the C2+ products and activity are sensitive to the surface species of catalysts, the role of surface species in enhancing generation of C2+ products was explored by in situ SERS (Supporting Information, Figure S10). For the Cu-nr-O, two broad bands at 524 and 610 cm^{-1} were

observed (Figure 3A), which were attributable to the Cu_2O, indicating that Cu_2O existed in Cu-nr-O. This was consistent with the results of XAS. We can observe that the corresponding Raman features of Cu_2O disappeared at -0.2 V vs. RHE or below, indicating full reduction of Cu-nr-O to Cu. New bands appeared at -0.2 V vs. RHE or below during CO_2RR, the bands will be analyzed according to the different potentials in the following.

At -0.2 V vs. RHE or below, a well-defined bands appeared at 1064 cm^{-1} on Cu-nr-OR and Cu-nr during CO_2RR (Figure 3A and Supporting Information, Figure S11), which was attribution to CO_3^{2-},[12] becuase CO_2 can dissolve in the KOH electrolyte, forming a neutral-pH carbonate mixture. The intensity of the band became weak with the potential decrease, which is because the CO_2 can be reduced at negetive potential and the formation of CO_3^{2-} become slow.

At -0.3 V vs. RHE or below, an additional band appeared at 524 cm^{-1} for Cu-nr-OR and Cu-nr during CO_2RR. According to the previous report,[39] the band can be assingned CuO_x or CuO_xOH_y species. When conducting in D_2O instead of H_2O, the band at 524 cm^{-1} displayed a negligible shift (Supporting Information, Figure S12), indicating that the band was attributed to CuO_x species rather that the CuO_xOH_y. There are three possible reasons for formation of CuO_x species (Figure 3C): (1) the CuO_x species were from the original Cu_2O; (2) from the reaction between reduced Cu and H_2O; and (3) from the reaction between reduced Cu and CO_2.

To address these concerns, ^{18}O isotope labeling experiments were carried out to confirm the source of oxygen in CuO_x. First, ^{18}O enriched Cu-nr-O catalysts were synthesized by oxidation of Cu-nr in $H_2{}^{18}O$ electrolyte. The $Cu_2{}^{18}O$ was formed in the Cu-nr-O, the bands were 504 and 590 cm^{-1} (Figure 3B), which exhibited significant red-shift compared with the $Cu_2{}^{16}O$.[27] This result indicates that the bands of CuO_x species showed a significant red shift when the ^{16}O was replaced by ^{18}O, which can be an important indicator for exploring the oxygen source of CuO_x species. For the ^{18}O enriched Cu-nr-OR, the CuO_x was also formed at -0.3 V vs. RHE, and the band was still at 524 cm^{-1}, which displays a negligible shift compared with that of the Cu-nr-OR. The results suggest that the CuO_x species were not from the original $Cu_2{}^{18}O$. Thus it can be deduced that the CuO_x was produced during the CO_2RR. Due to both the H_2O and CO_2 can react with reduced Cu to form CuO_x species, the oxygen source of CuO_x species should be further studied. Furthermore, the Cu-nr-OR were tested in $H_2{}^{18}O$ during CO_2RR, we can observe that the band of CuO_x was still at 524 cm^{-1} (Supporting Information, Figure S13), which indicated that the CuO_x was not from the reaction between Cu and $H_2{}^{18}O$. Thus the last possible reason is reasonable, *i.e.*, the CuO_x was from the reaction between Cu and CO_2. Because the CO_2 reduction is slow at -0.3 V vs. RHE and the signal of CO cannot be observed in raman spectra, we can assume that the CuO_x species were from the chemisorption of CO_2 on Cu. To further verify this argument, the electrolysis experiment over Cu-nr-OR

was tested under N_2 atmosphere, no bands were observed at negative potential (Supporting Information, Figure S14), indicating that the CO_2 played the key role for the formation of CuO_x species.

From the above results, we can deduce that the CuO_x existed during CO_2RR was just the singal of chemisorption of CO_2 on Cu, which was not the main factor for facilitating C2+ products during CO_2RR. In order to further verify this conclusion, the commercial Cu nanoparticles (about 50 nm) were also studied by in situ SERS (Supporting Information, Figure S15). It was shown that the CuO_x appeared at -0.3V vs. RHE or below (Supporting Information, Figure S16), which was similar to that of Cu-nr-OR, thus the CuO_x species were not specific for the Cu oxide derived catalysts.

At -0.4 V vs. RHE or below, for both the Cu-nr and Cu-nr-OR, the presence of adsorbed *CO on Cu was demonstrated by the appearance of Raman peaks located at 276, 360, and 2000-2100 cm^{-1}, which correspond to the restricted rotation of adsorbed *CO on Cu, Cu-CO stretching, and C≡O stretching, respectively (Figure 3A, and Supporting Information, Figure S11).[40] It is interesting to note that the band of C≡O stretching on Cu-nr-OR is different from that on Cu-nr (Figure 3D). A new peak appeared at about 2000 cm^{-2} on Cu-nr-OR compared with the Cu-nr. Specifically, the stretch mode of surface-adsorbed CO can serve as a molecular probe of surface structure due to its sensitivity to the structure of adsorption sites.[41-42] Thus, we can assume that new active sites were produced on Cu-nr-OR. It is reasonable to analyze the active sites using the surface-adsorbed CO at -0.4 V vs. RHE, becuase the C-C coupling step is slow at this potential. According to previous report,[43] different CO adsorption sites exhibit distinct catalytic behavior for the C-C coupling step, thus we can suppose that the enhanced generation of C2+ products over Cu-nr-OR was originated mainly from the formation of new active sites.

After the potential was removed, we could observe that the Cu_2O was formed rapidly (Supporting Information, Figure S17), indicating that the reduced Cu can be oxidized in electrolyte. Cu_2O can be formed via oxidation of Cu by the O_2 in electrolyte.[27] However, the content of O_2 is very low in the cathodic electrolyte. It is interesting to note that the $Cu_2{}^{18}O$ was formed when using $H_2{}^{18}O$ as electrolyte after the potential was removed (Supporting Information, Figure S18). Thus we can assume that the Cu_2O was from the reaction between Cu and H_2O. After the potential was removed, the reduced Cu was very active, which could react with the H_2O. The results indicate that the in situ method has obvious advantage and is necessary to explore the real state of the catalyst in the reaction.

Due to the coordination environment of Cu can alter the adsorption of CO and the energy barrier of C-C coupling step, we used operando XAS to monitor the local structure of Cu-nr and Cu-nr-OR during CO_2RR. For both catalysts, only peaks corresponding to metallic Cu were observed at negative potential during CO_2RR (Figure 4A, B and Supporting Information, Figure S19-S20), indicating that the CuO or Cu_2O was reduced to metallic Cu in CO_2RR. Moreover, the quantified Cu-Cu coordination number of the Cu-nr-OR and Cu-nr were fit using the ARTEMIS programs of IFEFFIT during CO_2RR (Supporting Information, Figure S21-

S22 and Table S2). No obvious difference of Cu-Cu coordination number was observed for the Cu-nr-OR and Cu-nr during CO_2RR, indicating that the enhancing of C2+ products over Cu-nr-OR was not mainly from the slight change of the coordinate environment.

The surface structure of the catalysts can be probed by electrosorption of hydroxide (OH_{ads}).[44] Qualitatively, for the Cu-nr, the intensity of (111) OH_{ads} feature was higher than that of (100) and (110), which suggests a high surface density of (111) on Cu-nr (Figure 4C). In contrast, for the Cu-nr-OR, the intensity of (111) OH_{ads} peak is reduced, which reflects that the proportions of (100) and (110) on Cu-nr-OR surface were higher that on Cu-nr. According to previous report,[32, 45] the (100) facet was favorable crystal orientation for the C-C coupling process. And the CO dimerization reaction (Figure 4D, and Supporting Information, Figures S23-25, Table S3) on Cu (111) and Cu (100) were investigated by DFT calculation, which is crucial for producing C2+ products.[46-49] The Cu (100) exhibited lower energy barrier for CO dimerization compared to Cu (111) (Figure 4E), suggesting that Cu (100) can enhance the formation of C2+ products. Thus, the increased Cu (100) facet can be considered as the main factor for enhancing C2+ products over Cu-nr-OR.

In summary, the surface species and structure over OD-Cu catalysts were systematically investigated by in situ SERS, operando XAS, and ^{18}O isotope labeling experiments combined with theoritical calculation. It was showed that the Cu oxides indeed existed on the surface of catalysts at during CO_2RR. However, they were formed by chemisorption of CO_2 on Cu instead of the active sites of the catalyst. The redox cycling treatment could create active Cu (100) facet, and DFT calculations suggested that the Cu (100) active facets could decrease the energy barrier of C-C coupling step, and enhancing C2+ products. In addition, this work also shows that in situ techniques have obvious advantages and are sometimes necessary to explore the structure of the catalyst and surface species in CO_2RR. We believe that the findings of this work provide useful knowledge for designing other efficient electrocatalysts for CO_2 reduction.

Methods

Materials. $Cu(NO_3)_2$ (99%), NaOH (98%), ammonium hydroxide (30%), and Ni foam were obtained from Sinopharm Chem. Reagent Co. Ltd. KOH (98%), sodium 2, 2-dimethyl-2-silapentane-5-sulfonate (DSS, 99%) and phenol were purchased from Alfa Aesar China Co., Ltd. D_2O (99.8% D) and $H_2{}^{18}O$ (97% ^{18}O) were purchased from Innochem Co., Ltd. N_2 (99.999%) and CO_2 (99.999%) were provided by Beijing Analytical Instrument Company. Deionized water was used in the experiments.

Synthetic procedures for Cu-nr. The Cu-nr was prepared by electroreduction of the CuO nanorods (CuO-nr) for 10 min at -0.9 V vs. RHE. CuO-nr was fabricated through the annealing of $Cu(OH)_2$ nanorods under N_2 atmosphere. The $Cu(OH)_2$ nanorods were prepared by a literature method.[23]

Synthetic procedures for Cu-nr-OR. The Cu-nr-OR was prepared by electroreduction of the Cu-nr-O for 10 min at -0.9 V vs. RHE. Firstly, the Cu-nr-O was prepared by electrochemical cycling of Cu-nr in 1.0 M KOH solutions. The experiment was performed in multi-potential steps mode. The potential and time for the step 1 was 1.0 V vs. RHE and 2s; the potential and time for the step 2 was 0.4 V vs. RHE and 1s; Then the Cu-nr-O was obtained after 20 cycles. Secondly, the Cu-nr-OR was prepared by electroreduction of the Cu-nr-O for 10 min at -0.9 V vs. RHE, and the electrolytewas 1M KOH solution.

Characterization. The SEM and TEM characterizations were carried out using a HITACHI S-4800 and JEOL JEM-2100F, equipped with EDS. The operando X-ray adsorption spectroscopy (XAS) measurements were performed using a modified flow cell at the 1W1B, 1W2B beamline at Beijing Synchrotron Radiation Facility (BSRF). In situ Raman measurements were carried out using a Horiba LabRAM HR Evolution Raman microscope in a modified flow cell, which was produced by GaossUnion (Tianjin) Photoelectric Technology Company. A 785-nm laser was used and signals were recorded using a 20 s integration and by averaging two scans.

Electrochemical study. Electrochemical studies were conducted in an electrochemical flow cell which including a gas chamber, a cathodic chamber, and an anodic chamber, as reported in our previous work.[38] An anion exchange membrane (FumasepFAA-3-PK-130) was used to separate the anodic and cathodic chambers, and an Ag/AgCl electrode and Ni foam were used as the reference and counter electrodes, respectively. The electrolysis was conducted using a CHI 660e electrochemical workstation equipped with a high current amplifier CHI 680c. The measured potentials after iR compensation were rescaled to the RHE by E (versus RHE) = E (versus Ag/AgCl) + 0.209 V+0.0591V/pH×pH. For electrolysis studies, 1 M KOH was used as the electrolyte, and it was circulated through the cathodic and anodic chambers using peristaltic pumps at a rate of 20 mL min^{-1}. The flow rate of CO_2 gas through the gas chamber was controlled to be 20 sccm using a digital gas flow controller.

Declarations

Acknowledgements

The authors thank the National Key Research and Development Program of China (2017YFA0403101, 2017YFA0403003 and 2017YFA0403102), National Natural Science Foundation of China (21890761, 21733011 and 21533011), Beijing Municipal Science & Technology Commission (Z191100007219009), and Chinese Academy of Sciences (QYZDY-SSW-SLH013). The operando X-ray adsorption spectroscopy (XAS) measurements were performed using a flow cell at the 1W1B, 1W2B beamline at Beijing Synchrotron Radiation Facility (BSRF), China.

Author contributions

C.J.C. and B.X.H. proposed the project, designed the experiments and wrote the manuscript; C.J.C. performed the whole experiments; X.P.Y., Y.H.W., H.Z.L., X.F.S, Q.G.Z, T.B.W and Q.L.Q assisted in analyzing

the experimental data; F.R.J assisted in analyzing the experimental data of In situ SERS; S.J.L, J.Z and L.R.Z assisted in analyzing the experimental data of XAS; B.X.H. supervised the whole project.

Additional information

Supplementary information is available in the online version of the paper. Reprints and permissions information is available online at www.nature.com/reprints. Correspondence and requests for materials should be addressed to B.X.H.

Competing financial interests

The authors declare no competing financial interests.

References

1. Wang, H. *et al.*, Synergistic enhancement of electrocatalytic CO_2 reduction to C2 oxygenates at nitrogen-doped nanodiamonds/Cu interface. *Nanotechnol* **15**, 131-137 (2020).
2. He, M. Sun, Y. Han, B. Green carbon science: scientific basis for integrating carbon resource processing, utilization, and recycling. *Chem. Int. Ed.* **52**, 9620-9633 (2013).
3. Gu, J. *et al.*, Atomically dispersed Fe^{3+} sites catalyze efficient CO_2 electroreduction to CO. *Science* **364**, 1091-1094 (2019).
4. Chen, C. *et al.*, Boosting CO_2 Electroreduction on N, P-Co-doped Carbon Aerogels. *Chem. Int. Ed.* **59**, 11123-11129 (2020).
5. Nwabara, U. O. Cofell, E. R. Verma, S. Negro, E. Kenis, P. J. A. Durable Cathodes and Electrolyzers for the Efficient Aqueous Electrochemical Reduction of CO_2. *ChemSusChem* **13**, 855-875 (2020).
6. De, R. *et al.*, Electrocatalytic Reduction of CO_2 to Acetic Acid by a Molecular Manganese Corrole Complex. *Chem. Int. Ed.* **59**, 10527-10534 (2020).
7. Wang, X. *et al.*, Efficient electrically powered CO_2-to-ethanol via suppression of deoxygenation. *Nature Energy* **5**, 478-486 (2020).
8. Wang, X. *et al.*, Mechanistic reaction pathways of enhanced ethylene yields during electroreduction of CO_2-CO co-feeds on Cu and Cu-tandem electrocatalysts. *Nanotechnol* **14**, 1063-1070 (2019).
9. Ma, W. *et al.*, Electrocatalytic reduction of CO_2 to ethylene and ethanol through hydrogen-assisted C-C coupling over fluorine-modified copper. *Catal.* **3**, 478-487 (2020).
10. Wang, H. *et al.*, Rapid and Scalable Synthesis of Cuprous Halide-Derived Copper Nano-Architectures for Selective Electrochemical Reduction of Carbon Dioxide. *Nano Lett.* **19**, 3925-3932 (2019).
11. Fan, L. *et al.*, Strategies in catalysts and electrolyzer design for electrochemical CO_2 reduction toward C2+ products. *Adv.* **6**, eaay3111 (2020).
12. Vasileff, A. *et al.*, Electrochemical Reduction of CO_2 to Ethane through Stabilization of an Ethoxy Intermediate. *Chem. Int. Ed.* doi: 10.1002/anie.202004846.

13. Zheng, Y. *et al.*, Understanding the Roadmap for Electrochemical Reduction of CO_2 to Multi-Carbon Oxygenates and Hydrocarbons on Copper-Based Catalysts. *Am. Chem. Soc.* **141**, 7646-7659 (2019).
14. Gao, D. Arán-Ais, R. M. Jeon, H. S. Cuenya, B. R. Rational catalyst and electrolyte design for CO_2 electroreduction towards multicarbon products. *Catal.* **2**, 198-210 (2019).
15. Wu, J. *et al.*, A metal-free electrocatalyst for carbon dioxide reduction to multi-carbon hydrocarbons and oxygenates. *Commun.* **7**, 13869 (2016).
16. Grosse, P. *et al.*, Dynamic Changes in the Structure, Chemical State and Catalytic Selectivity of Cu Nanocubes during CO_2 Electroreduction: Size and Support Effects. *Chem. Int. Ed.* **57**, 6192-6197 (2018).
17. Gao, D. *et al.*, Selective CO_2 Electroreduction to Ethylene and Multicarbon Alcohols via Electrolyte-Driven Nanostructuring. *Chem. Int. Ed.* **58**, 17047-17053 (2019).
18. Raciti, D. Wang, C. Recent Advances in CO_2 Reduction Electrocatalysis on Copper. *ACS Energy Lett.* **3**, 1545-1556 (2018).
19. Kim, D. Kley, C. S. Li, Y. Yang P., Copper nanoparticle ensembles for selective electroreduction of CO_2 to C2-C3 products. *Natl. Acad. Sci. USA* **114**, 10560-10565 (2017).
20. Li , Y. *et al.*, Electrochemically scrambled nanocrystals are catalytically active for CO2-to-multicarbons. *Natl. Acad. Sci. USA* **117**, 9194-9201 (2020).
21. Gao, D. *et al.*, Activity and Selectivity Control in CO_2 Electroreduction to Multicarbon Products over CuOx Catalysts via Electrolyte Design. *ACS Catal.* **8**, 10012-10020 (2018).
22. Zhu, Q. *et al.*, Carbon dioxide electroreduction to C2 products over copper-cuprous oxide derived from electrosynthesized copper complex. *Commun.* **10**, 3851 (2019).
23. Lv, J. J. *et al.*, A Highly Porous Copper Electrocatalyst for Carbon Dioxide Reduction. *Mater.* **30**, e1803111 (2018).
24. Gao, D. *et al.*, Plasma-Activated Copper Nanocube Catalysts for Efficient Carbon Dioxide Electroreduction to Hydrocarbons and Alcohols. *ACS Nano* **11**, 4825-4831 (2017).
25. Mistry, H. *et al.*, Highly selective plasma-activated copper catalysts for carbon dioxide reduction to ethylene. *Nat Commun* **7**, 12123 (2016).
26. Eilert, A. *et al.*, Subsurface Oxygen in Oxide-Derived Copper Electrocatalysts for Carbon Dioxide Reduction. *Phys. Chem. Lett.* **8**, 285-290 (2017).
27. Lum, Y. Ager, J. W. Stability of Residual Oxides in Oxide-Derived Copper Catalysts for Electrochemical CO_2 Reduction Investigated with (18) O Labeling. *Chem. Int. Ed.* **57**, 551-554 (2018).
28. Dinh, -T. *et al.*, CO_2 electroreduction to ethylene via hydroxide-mediated copper catalysis at an abrupt interface. *Science 360*, 783-787 (2018).
29. Arán-Ais, R. M. Scholten, F. Kunze, S. Rizo, R. Roldan Cuenya, B. The role of in situ generated morphological motifs and Cu(i) species in C2+ product selectivity during CO_2 pulsed electroreduction. *Nature Energy* **5**, 317-325 (2020).

30. Yang, P.-P. *et al.*, Protecting Copper Oxidation State via Intermediate Confinement for Selective CO_2 Electroreduction to C2+ Fuels. *Am. Chem. Soc.* **142**, 6400-6408 (2020).
31. Tomboc, G. M. Choi, S. Kwon, T. Hwang, Y. J. Lee, K. Potential Link between Cu Surface and Selective CO_2 Electroreduction: Perspective on Future Electrocatalyst Designs. *Mater.* **32**, e1908398 (2020).
32. Chen, C. *et al.*, A strategy to control the grain boundary density and Cu^+/Cu^0 ratio of Cu-based catalysts for efficient electroreduction of CO_2 to C2 products. *Green Chem.* **22**, 1572-1576 (2020).
33. Wang, Y. *et al.*, Catalyst synthesis under CO_2 electroreduction favours faceting and promotes renewable fuels electrosynthesis. *Catal.* **3**, 98-106 (2020).
34. Kim, J. *et al.*, Branched Copper Oxide Nanoparticles Induce Highly Selective Ethylene Production by Electrochemical Carbon Dioxide Reduction. *Am. Chem. Soc.* **141**, 6986-6994 (2019).
35. Lei, Q. *et al.*, Investigating the Origin of Enhanced C2+ Selectivity in Oxide-/Hydroxide-Derived Copper Electrodes during CO_2 *J. Am. Chem. Soc.* **142**, 4213-4222 (2020).
36. Randle, V. Rohrer, G. S. Miller, H. M. Coleman, M. Owen, G. T. Five-parameter grain boundary distribution of commercially grain boundary engineered nickel and copper. *Acta Mater.* **56**, 2363-2373 (2008).
37. Medlin, D. L. Hattar, K. Zimmerman, J. A. Abdeljawad, F. Foiles, S. M. Defect character at grain boundary facet junctions: Analysis of an asymmetric Σ = 5 grain boundary in Fe. *Acta Mater.* **124**, 383-396 (2017).
38. Chen, C. *et al.*, Highly Efficient Electroreduction of CO_2 to C2+ Alcohols on Heterogeneous Dual Active Sites. *Chem. Int. Ed.* doi.org/10.1002/anie.202006847.
39. Zhao, Y. *et al.*, Speciation of Cu Surfaces During the Electrochemical CO Reduction Reaction. *Am. Chem. Soc.* **142**, 9735-9743 (2020).
40. Gao, J. *et al.*, Selective C-C Coupling in Carbon Dioxide Electroreduction via Efficient Spillover of Intermediates As Supported by Operando Raman Spectroscopy. *Am. Chem. Soc.* **141**, 18704-18714 (2019).
41. Eren, B. Liu, Z. Stacchiola, D. Somorjai, G. A. Salmeron, M. Structural Changes of Cu(110) and Cu(110)-(2 × 1)-O Surfaces under Carbon Monoxide in the Torr Pressure Range Studied with Scanning Tunneling Microscopy and Infrared Reflection Absorption Spectroscopy. *Phys. Chem. C* **120**, 8227-8231 (2016).
42. Gunathunge, C. M. *et al.*, Spectroscopic Observation of Reversible Surface Reconstruction of Copper Electrodes under CO_2 *J. Phys. Chem. C* **121**, 12337-12344 (2017).
43. Gunathunge, C. M. Ovalle, V. J. Li, Y. Janik, M. J. Waegele, M. M. Existence of an Electrochemically Inert CO Population on Cu Electrodes in Alkaline pH. *ACS Catal.* **8**, 7507-7516 (2018).
44. Luc, W. *et al.*, Two-dimensional copper nanosheets for electrochemical reduction of carbon monoxide to acetate. *Catal.* **2**, 423-430 (2019).
45. Hori, Y. Takahashi, I. Koga, O. Hoshi, N. Electrochemical reduction of carbon dioxide at various series of copper single crystal electrodes. *J. Mol. Catal. A: Chem.* **199**, 39-47 (2003).

46. Schouten, K. J. Qin, Z. Perez Gallent, E. Koper, M. T. Two pathways for the formation of ethylene in CO reduction on single-crystal copper electrodes. *Am. Chem. Soc.* **134**, 9864-9867 (2012)
47. Calle-Vallejo, F. Koper, M. T. M. Theoretical Considerations on the Electroreduction of CO to C2 Species on Cu(100) Electrodes. *Chem. Int. Ed.* **52**, 7282-7285 (2013).
48. Montoya, J. H. Shi, C. Chan, K. Norskov, J. K. Theoretical Insights into a CO Dimerization Mechanism in CO_2 *J. Phys. Chem. Lett.* **6**, 2032-2037 (2015).
49. Montoya, J. H. Peterson, A. A. Nørskov, J. K. Insights into C≡C Coupling in CO_2 Electroreduction on Copper Electrodes. *ChemCatChem* **5**, 737-742 (2013).

Figures

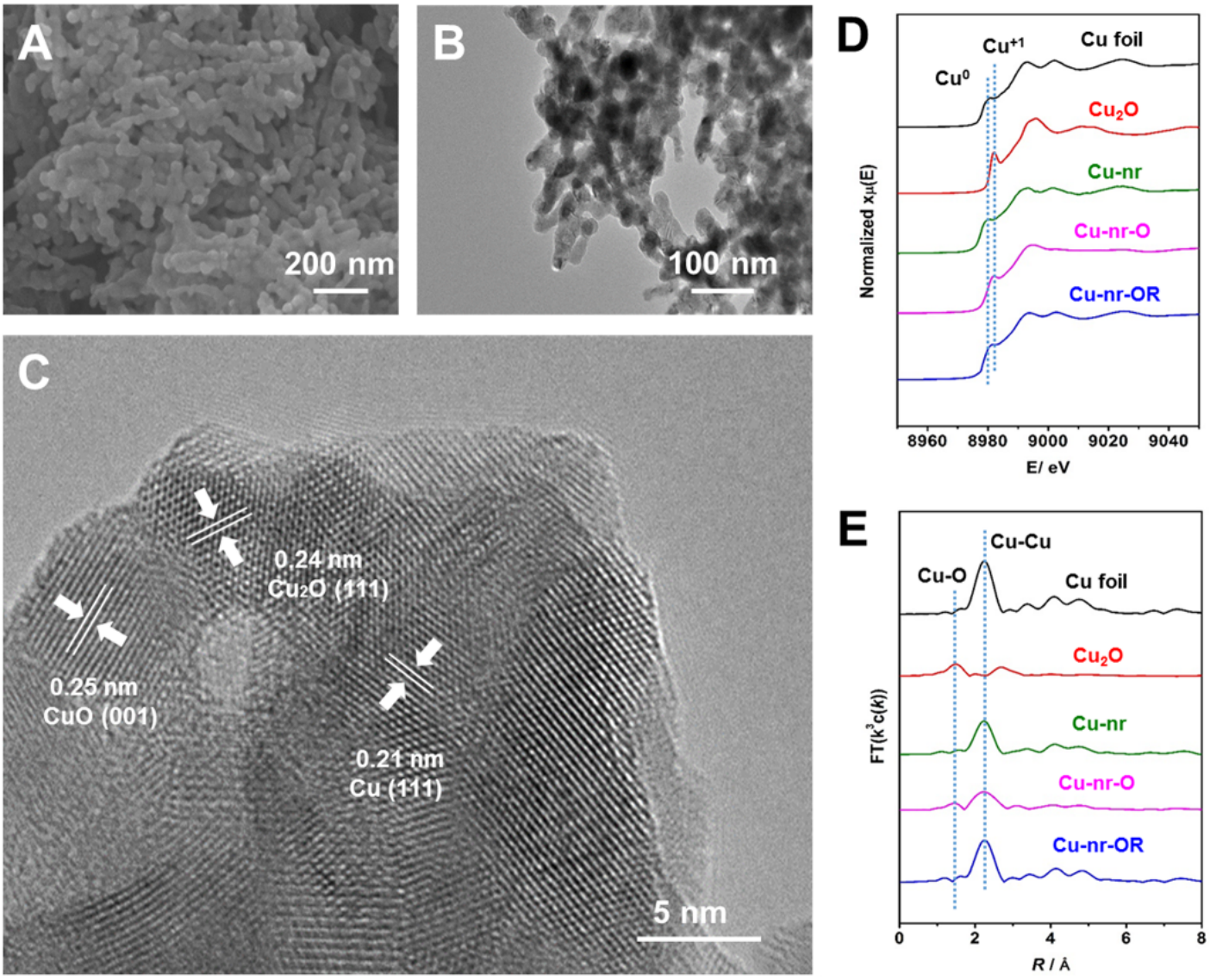

Figure 1

(A, B) The SEM and TEM images of the Cu-nr-OR. (C) HR-TEM image of the Cu-nr-OR. (D) The XANES spectra at the Cu K-edge for different catalysts. (E) Fourier-transformed Cu K-edge EXAFS spectra for different catalysts.

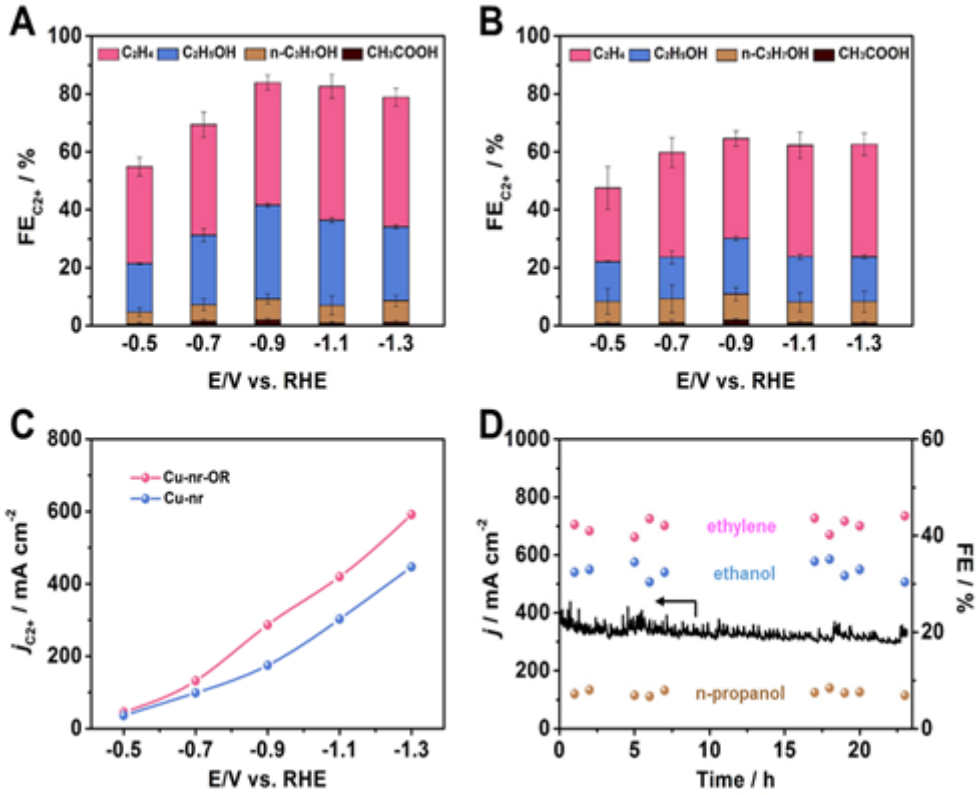

Figure 2

(A) The distribution of C2+ products at different potentials over Cu-nr-OR. (B) The distribution of C2+ products at different potentials over Cu-nr. (C) The partial current density of C2+ products at different potentials for the two catalysts. (D) Long-term stability of Cu-nr- OR at -0.9 V vs. RHE for 24 h.

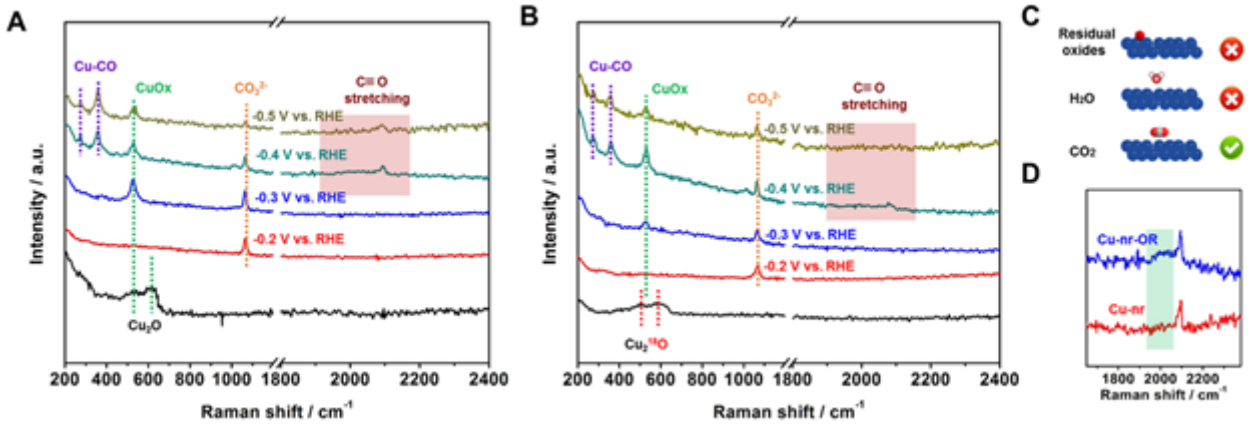

Figure 3

(A) The in-situ surface-enhanced Raman spectra for Cu-nr-OR at different potentials during CO2RR. (B) The in-situ surface-enhanced Raman spectra for 18O enriched Cu-nr-O at different potentials during CO2RR. (C) The schematic illustration of the possible reasions for formation of CuOx species during CO2RR. (D) The local enlarged view of the in-situ surface-enhanced Raman spectra for Cu-nr and Cu-nr-OR at -0.4V vs.RHE during CO2RR.

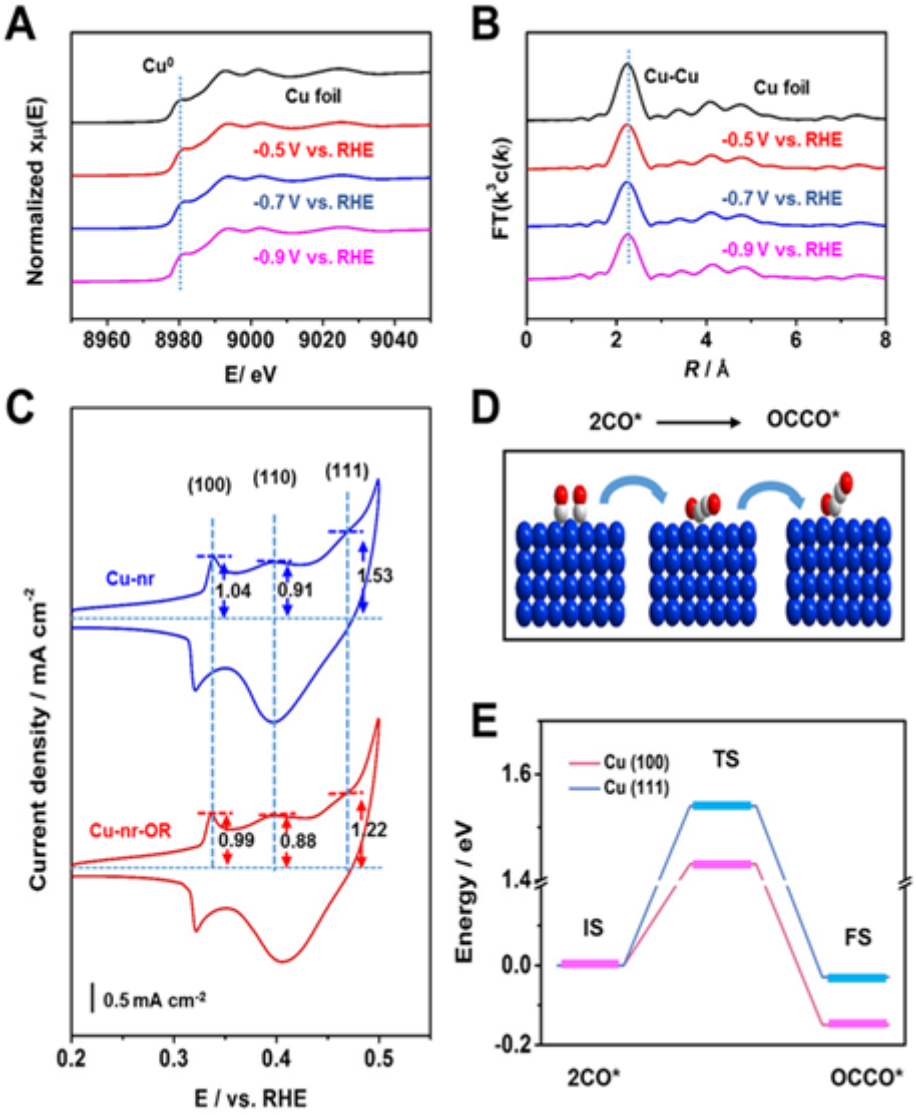

Figure 4

(A) The operando XANES spectra at the Cu K-edge for Cu-nr-OR at different potentials during CO2RR. (B) The corresponding Fourier transforms FT(k3w(k)) for Cu-nr-OR at different potentials during CO2RR. (C) The Voltammograms of OHads peaks for Cu-nr and Cu-nr-OR. (D) The schematic illustration of the CO dimerization on Cu. (E) Energy profiles for initial states (ISs), transition states (TSs), and final states (FSs) of CO dimerization on different crystal facets.

Supplementary Files

This is a list of supplementary files associated with this preprint. Click to download.

- supplement1.docx